SMiRT-12 / K. Kussmaul (Editor)

L07/1

INELASTIC DEFORMATION AND FATIGUE UNDER COMPLEX LOADING

C.H. Wang and M.W. Brown

Department of Mechanical & Process Engineering, The University of Sheffield, Mappin Street, Sheffield S1 3JD, UK

ABSTRACT

This paper presents an experimental and theoretical investigation of deformation and fatigue behaviour under multiaxial random loading. The inelastic stress-strain response under complex loading paths has been predicted using an incremental plasticity model, which incorporates a memory rule. Based on hysteresis strain hardening behaviour and the history described by the memory effect under multiaxial loading, a strain-based cycle counting method has also been proposed for multiaxial random loading. The evaluation of cumulative damage by the cycle counting method combined with Miner's linear rule and a strain-path dependent fatigue damage parameter is compared with experimental results under biaxial variable amplitude loading.

1 INTRODUCTION

Fatigue under multiaxial random loading is of great importance to engineers and designers, since many engineering structures and components in service are frequently subjected to complex loading. Some examples are nuclear reactors, pressure vessels, gas turbines, crankshafts, and so on. Fatigue failure or fracture may arise as a result of crack extension, which may be associated with metallurgical changes, in the highly stressed regions in these structures and components. A primary prerequisite to the analysis of integrity and safety assessment under these circumstances is the assimilation of the stress/strain state at critical sites into an equivalent strain measure. Hence a simple yet effective constitutive model and an associated fatigue life prediction method are required, which could be used by engineers in routine design and analyses.

A number of plasticity models [1-3] have been developed over the last two decades to estimate material behaviour under complex loading, which have been described in a review [4] and a recent state of the art publication [5]. However, many of these models have complex mathematical formulations and therefore, a large number of material constants are required to achieve reasonable simulation of the non-proportional loading effect. Consequently the simplicity and physical clarity desired may be lost, and it becomes difficult to relate these models to the fatigue damage mechanisms under multiaxial loading. The lack of fundamental

understanding of non-proportional hysteresis hardening has contributed partially to the non-existence of viable multiaxial cycle counting and fatigue damage prediction methods.

Although extensive studies have been carried out on fatigue under constant amplitude multiaxial loading, these models, being whether strain, stress, or energy based, are virtually useless for multiaxial random loading, unless the load history is entirely proportional (i.e. a constant stress/strain state). A suitable cycle counting method is needed to extend these models to general multiaxial random loading. A life prediction method was proposed in ASME Boiler and Pressure Vessel Code N-47-11 [6] to calculate the equivalent strain range for a single cycle of non-proportional loading, but the procedure does not render a cycle counting method. Each cycle must be closed, that is the starting and ending conditions of the cycle (principal axes, strain values and strain state) must be identical. The identification of a well-defined equivalent history is possible for a sequence of closed cycles, permitting a cycle by cycle application of Miner's linear summation rule to predict fatigue damage.

The aim of the present work is to study the effect of loading path on deformation and fatigue behaviour, and to develop a physically based cycle counting method suitable for non-proportional variable amplitude loading. A plasticity model and a memory rule have been proposed, and are shown to be capable of predicting the inelastic deformation under complex loading. This provides a theoretical basis for a multiaxial cycle counting method, whose capability has been demonstrated by a comparison between experimental results and predictions for two materials.

2 MODELLING OF HYSTERESIS HARDENING

To model deformation response under multiaxial random loading, it is essential to study hysteresis strain hardening and its dependence on loading history, which is reflected in the inheritance and erasing of memories under cyclic variable amplitude loading. Rainflow [7] and range pair [8] cycle counting methods have been widely accepted as the best methods of estimating fatigue damage under uniaxial random loading. The success of rainflow and range pair methods is mainly due to their ability to identify closed hysteresis loops as cycles; this is because the cyclic plastic deformation induced by dislocation movement provides the driving force for fatigue failure. Therefore hysteresis strain hardening behaviour should provide a basis for developing multiaxial cycle counting procedures.

Here we define the relative stresses ($\boldsymbol{\sigma}^*$) and strains ($\boldsymbol{\epsilon}^*$) as the differences between the instantaneous stresses or strains and those at the previous turning point,

$$\boldsymbol{\sigma}^* = \boldsymbol{\sigma} - \boldsymbol{\sigma}^R \tag{1}$$

$$\boldsymbol{\epsilon}^* = \boldsymbol{\epsilon} - \boldsymbol{\epsilon}^R \tag{2}$$

where the superscript R denotes the stress or strain tensor at that turning point. The equivalent relative stress and strain are defined for either von MISES or TRESCA type criteria, e.g. for equivalent relative strain,

$$\epsilon^*_{eq} = \begin{cases} \sqrt{(3/2)\boldsymbol{e}^* : \boldsymbol{e}^*}/(1+\nu') & \text{von MISES type} \\ \max(\gamma_1^*, \gamma_2^*, \gamma_3^*)/(1+\nu') & \text{TRESCA type} \end{cases} \tag{3}$$

where the tensor $\boldsymbol{e}^*$ [$= \boldsymbol{\epsilon}^* - \boldsymbol{I}\mathrm{Tr}(\boldsymbol{\epsilon})/3$] is the deviatoric relative strain tensor, and γ_i^* ($i = 1, 2, 3$) are the principal values of the relative shear strains. Here ν' is the effective Poisson's ratio. In a similar way we can also define an equivalent relative stress.

The constitutive model presented below adopts two surfaces, a stationary limit surface and a loading surface which may translate in the stress space inside the limit surface [9].

$$\text{Loading surface:} \qquad f \equiv F(\boldsymbol{S}-\boldsymbol{\alpha}) - \sigma_y^2 = 0 \tag{4}$$

$$\text{Limit surface:} \qquad \psi \equiv F(\boldsymbol{S}^L) - L^2 = 0 \tag{5}$$

where $\boldsymbol{S}$ and $\boldsymbol{\alpha}$ represent the current stress state and the centre of the loading surface in deviatoric stress space, or the deviatoric back stress. The tensor $\boldsymbol{S}^L$ represents a generic point on the limit surface. The quantities $\sqrt{2/3}\sigma_y$ and $\sqrt{2/3}L$ are the radii of the loading and limit surfaces in deviatoric stress space, respectively. The plastic flow follows the normality rule,

$$\dot{\boldsymbol{\epsilon}}^p = \begin{cases} (1/h)(\dot{\boldsymbol{S}}:\boldsymbol{n})\boldsymbol{n} & \text{if } f=0 \text{ and } \partial f/\partial \boldsymbol{S}:\boldsymbol{S} \geq 0 \\ \boldsymbol{0} & \text{otherwise} \end{cases} \tag{6}$$

where h is a generalized plastic modulus which will be discussed later, and $\boldsymbol{n}$ is the unit normal to the loading surface $f=0$ at point $\boldsymbol{S}$, which can be expressed as $\partial f/\partial \boldsymbol{S}/||\partial f/\partial \boldsymbol{S}||$. Here the usual decomposition of the total strain into elastic and plastic components is assumed, i.e., $\dot{\boldsymbol{\epsilon}} = \dot{\boldsymbol{\epsilon}}^e + \dot{\boldsymbol{\epsilon}}^p$. In what follows we will use a von MISES type of criterion for simplicity, so,

$$F = (3/2)\boldsymbol{S}:\boldsymbol{S} \tag{7}$$

We define an image point, $\boldsymbol{S}^L$, on the limit surface $\psi = 0$ which has the same outward normal as the normal, $\boldsymbol{n}$, to the loading surface at the current stress state,

$$\boldsymbol{S}^L = L(\boldsymbol{S}-\boldsymbol{\alpha})/\sigma_y = \sqrt{\frac{2}{3}}L\boldsymbol{n} \tag{8}$$

where $\boldsymbol{n} = \sqrt{3}(\boldsymbol{S}-\boldsymbol{\alpha})/(\sqrt{2}\sigma_y)$ represents the unit normal of the loading surface.

A general kinematic hardening rule can be expressed as,

$$\dot{\boldsymbol{\alpha}} = \boldsymbol{A}\dot{\mu} \tag{9}$$

where $\boldsymbol{A}$ represents the direction in which the centre of loading surface translates, and three popular hardening rules can be written as,

$$\boldsymbol{A} = \begin{cases} \boldsymbol{n} & \text{Prager rule [10]} \\ (\boldsymbol{S}^L - \boldsymbol{S}) = \sqrt{\frac{2}{3}}(L-\sigma_y)\boldsymbol{n} - \boldsymbol{\alpha} & \text{Mroz rule [1]} \\ \boldsymbol{n} - \gamma\boldsymbol{\alpha} & \text{Armstrong-Frederick (AF) rule [11]} \end{cases} \tag{10}$$

Here the coefficient $\dot{\mu}$ can be obtained from the consistency condition, i.e. $f \equiv 0$ holds during plastic loading,

$$\dot{\mu} = \frac{(\partial f/\partial \boldsymbol{S}):\dot{\boldsymbol{S}}}{(\partial f/\partial \boldsymbol{S}):\boldsymbol{A}} \tag{11}$$

Equation (10) implies that both Prager and Mroz rules can be considered as two special cases of the AF rule, with $\gamma = 0$ and $\sqrt{3}/(\sqrt{2}(L-\sigma_y))$ for Prager and Mroz rules, respectively. As

the freedom of the original AF rule is limited, some researchers (see Ref. [5]) have argued that multiple back stresses (consequently multiple material constants) have to be used in order to achieve good correlation with experimental data, although these approaches are subjected to the suspicion of "curve fitting". The comparison between experimental data and predictions showed that Prager's rule is inferior to the Mroz rule for non-proportional loading. In the present work we will use a Mroz kinematic hardening rule for its simplicity and geometrical consistency. Unfortunately the Mroz hardening rule does not allow ratchetting under mean stress cycling unless the loading is non-proportional. Since we are mainly concerned with strain-controlled fatigue loading, ratchetting is not a major issue.

To efficiently implement the model in computer code, a consistency condition in finite difference form is desired to avoid the use of radial return or iteration calculation procedures. After a load increment, $d\boldsymbol{S}$, the centre of the loading surface translates according to equation (10), and we have,

$$\begin{aligned} f &\equiv (3/2)(\boldsymbol{S}+d\boldsymbol{S}-\boldsymbol{\alpha}-d\boldsymbol{\alpha}):(\boldsymbol{S}+d\boldsymbol{S}-\boldsymbol{\alpha}-d\boldsymbol{\alpha})-\sigma_y^2 \\ &\equiv (3/2)[\boldsymbol{A}:\boldsymbol{A}\ (d\mu)^2-2\boldsymbol{A}:\boldsymbol{B}\ d\mu+\boldsymbol{B}:\boldsymbol{B}]-\sigma_y^2=0 \end{aligned} \tag{12}$$

where $\boldsymbol{B}$ is equal to $\boldsymbol{S}-\boldsymbol{\alpha}+d\boldsymbol{S}$. Here $d\mu$ should take the smaller root of the two solutions of equation (12). This furnishes a simple method for numerical computation to update the back stress ($\boldsymbol{\alpha}$).

In the case of proportional loading, the hysteresis strain hardening or the shape of hysteresis loop can be represented in terms of equivalent stress and strain, $\epsilon^*_{eq}=f(\sigma^*_{eq})$. Here the function f may depend on loading history. When the Ramberg-Osgood relationship is used, three material parameters suffice to characterise the hysteresis hardening,

$$\epsilon^*_{eq}=\epsilon^*_{eq,e}+\epsilon^*_{eq,p}=\frac{\sigma^*_{eq}}{E}+\left(\frac{\sigma^*_{eq}}{H}\right)^{1/m} \tag{13}$$

where $\epsilon^*_{eq,e}$ and $\epsilon^*_{eq,p}$ represent the elastic and plastic components of the equivalent relative strain, and E is Young's modulus. The values of H and m in general may depend on material, loading history, and so on. For those materials obeying Masing's assumption, the hysteresis hardening coefficient (H) and exponent (m) are equal to the cyclic stress-strain hardening coefficient (K') and exponent (n'), respectively.

Here we introduce an internal variable, D, which is defined as the projection of the vector connecting the loading point and its image point on the normal to the loading surface (at the loading point),

$$D=\sqrt{\frac{3}{2}}(\boldsymbol{S}^L-\boldsymbol{S}):\boldsymbol{n}=L-\sqrt{\frac{3}{2}}\boldsymbol{S}:\boldsymbol{n} \tag{14}$$

It can be shown that for proportional loading the equivalent relative stress σ^*_{eq} is equal to $2L-D-D^R$. Hence the scalar multiplier h in equation (6) can be obtained by differentiating equation (13),

$$h=\frac{2}{3}E_p=\frac{2}{3}\frac{d\sigma^*_{eq}}{d\epsilon^*_{eq,p}}=\frac{2mH}{3}\left(\frac{\sigma^*_{eq}}{H}\right)^{1-1/m}=\frac{2mH}{3}\left(\frac{2L-D-D^R}{H}\right)^{1-1/m} \tag{15}$$

where D^R is a discrete memory variable which takes the value of D at the active memory point. Here the memory of loading history is represented by a one-dimensional array to

preserve the simplicity and physical clarity, although a second order or even higher rank of tensor may store more pertinent information than a one-dimensional array. This array encapsulates the interactive effects of the stable dislocation cell structure on the plastic flow stress.

The following memory rule is proposed for general multiaxial loading,

1. Strong memories will be produced when a plastic loading is followed by a complete unloading, or $(\boldsymbol{S}-\boldsymbol{\alpha}):(\boldsymbol{S}-\boldsymbol{\alpha})<0$, otherwise weak memories will be produced.

2. During plastic deformation, if value of D increases, then the current point is a weak memory which is also the active memory, otherwise:

   - Case 1: If the active memory ($D^R[n]$) is strong and D becomes less than $D^R[n-1]$, then two memories ($D^R[n]$ and $D^R[n\text{-}1]$) will be erased and the next memory in the stack $D^R[n\text{-}2]$ will be invoked to become active, whereas when $n \leq 2$ then the current point becomes the active memory point, viz $D^R[1] = D$.
   - Case 2: If the active memory ($D^R[n]$) is weak and D becomes less than $D^R[n]$, then the memory $D^R[n]$ will be erased and the next memory in the stack $D^R[n\text{-}1]$ will be activated.

One attractive feature of the proposed method is that it enables the effect of loading history to be modelled by a one-dimensional array ($D^R[n]$), which stores the memories created by turning points. The integration of the history memory variable with the hysteresis hardening modulus, h, combined with the loading surface provide the means for the description of the anisotropic hardening and complex memory effects resulting from successive loading and unloading in different directions. Fig.1 shows an example of proportional variable amplitude loading, where the solid line represents the predicted response and the symbols are recorded data for En15R steel under combined tension-torsion loading [9].

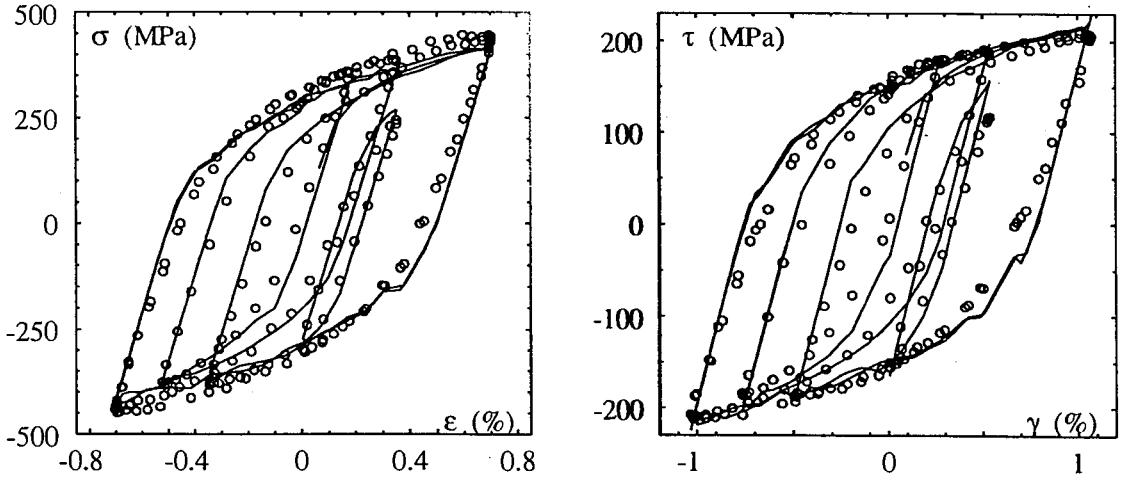

Fig 1: Deformation response under proportional variable amplitude loading (En15R)

One critical loading path which poses a serious challenge to many plasticity theories is the case of 90^0 out-of-phase loading with biaxiality $\gamma/\epsilon = 1.5$. This is the case that the loading

point tends to move in a direction tangential to the yield surface. The experimental data and theoretical predictions are shown in Fig.2, showing reasonable correlation, so long as a 14% correlation to the modulus H is included to account for cross-hardening (see Ref. [9]). In order to examine the memory rule and to further elucidate strong and weak memories, a prediction was performed with strong memories only, viz, removing the clauses on weak memories, so all memories are of strong type. The prediction is marked by the dashed curve, clearly both axial stress and shear stress are under-estimated as a result of the relatively higher value of D^R in equation (15). This demonstrates the important role of the weak memory and its capacity. An example of multiaxial random loading is shown in Fig.3, the predicted response exhibiting a good correlation with the experimental data. In all the three cases considered, not only have the maximum stresses been correctly predicted, but also the loop shapes of major and minor hysteresis curves have also been adequately simulated.

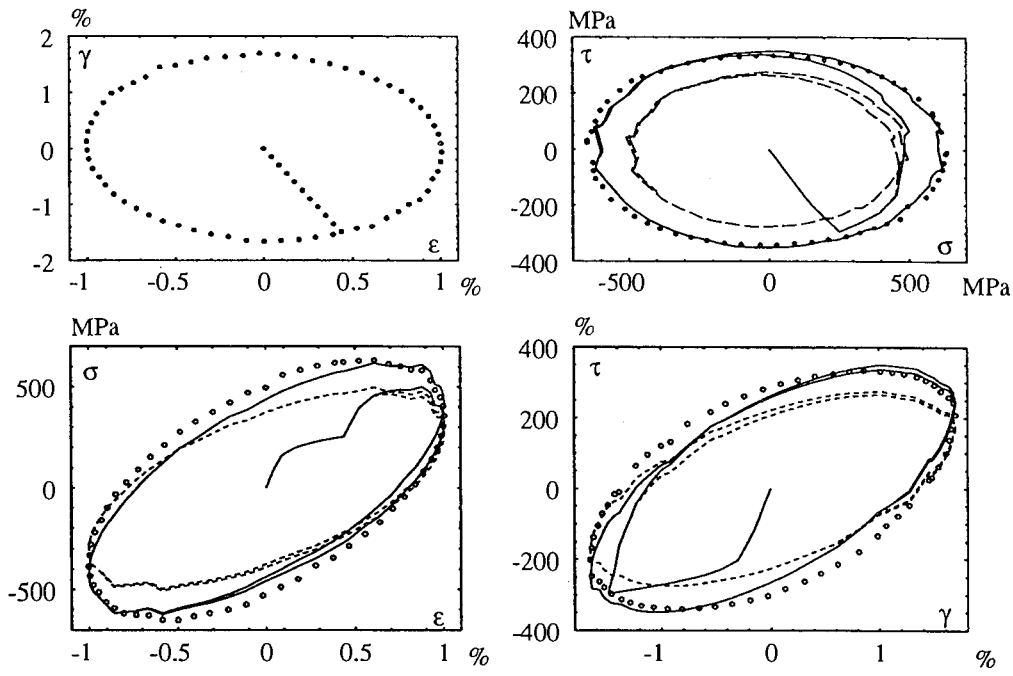

Fig 2: Deformation response under out-of-phase loading for En15R steel

3 MULTIAXIAL CYCLE COUNTING METHOD

Since it is the plastic deformation that is the driving force for fatigue damage, a general definition of reversal or turning point can be expressed as the event when the driving force attains peak value, which corresponds to a change in the direction of dislocation movement. In the case of radial (proportional) loading, a complete reversing of the dislocation flow occurs at a turning point, whereas in the case of non-proportional loading, the change may be gradual. For example in the case of 90^0 out-of-phase sinusoidal straining in combined tension/torsion tests, the maximum shear plane rotates gradually through the cycle without elastic unloading. One important implication of the memory rule presented in preceding section is that a "cycle" may not necessarily be closed for the case of non-proportional

variable amplitude loading. Nevertheless, when the equivalent relative strain attains its peak value, so does the equivalent stress, indicating that a complete change in dislocation dynamics occurs irrespective of the reference state. Therefore a half cycle can be counted between two relative peak points of the equivalent relative strain (or stress).

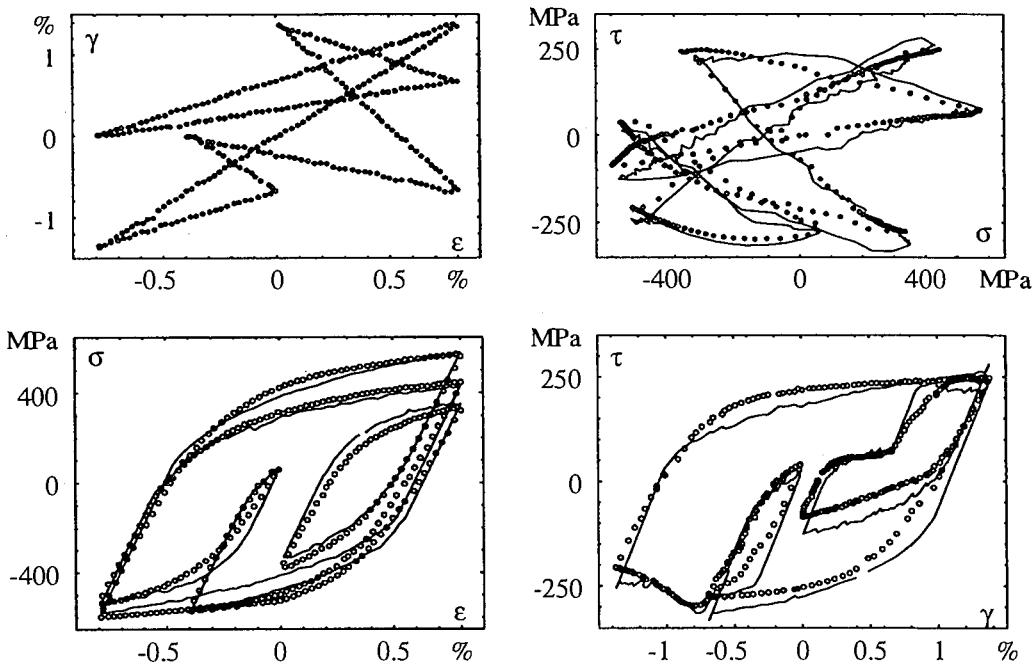

Fig 3: Deformation response under non-proportional variable amplitude loading (En15R)

Assuming the initial state of the material is at zero stress/strain state, the point at which the equivalent strain achieves peak value over the whole history would coincide with the most significant turning point, viz,

$$\epsilon_{eq\ (t=t_A)} = \max_{0\le t\le\theta} \epsilon_{eq}(\epsilon_{ij}(t)) \tag{16}$$

where time period $0 \le t \le \theta$ represents the loading block, and t_A is the major turning point, as shown in Fig.4a. Here the equivalent strain can be of TRESCA or von MISES type for materials which obey TRESCA or MISES yield criteria.

The original data block can now be rearranged to start with the major turning point; this can be done by moving the data within $[0, t_A]$ to the end of the block. Then plot the equivalent relative strain defined in equation (3) (where $\epsilon^R = \epsilon^A_{ij}$) with respect to time. The peak value of $\epsilon^*_{eq}(t)$ would register another turning point,

$$\epsilon_{eq\ (t=t_E)} = \max_{t_A\le t\le\theta+t_A} \epsilon_{eq}(\epsilon_{ij}(t) - \epsilon^A_{ij}) \tag{17}$$

where ϵ^A_{ij} are the strains at time t_A, and the time at which the peak value occurs is t_E (Fig.4b). The above expression is equivalent to considering the strains at a turning point as residual strains, and since mean or residual strain has little effect on crack growth, the relative strains $(\epsilon_{ij} - \epsilon^R_{ij})$ are thus the effective driving force for fatigue damage.

Since the value of ϵ^*_{eq} may not be monotonically increasing with time, each decrease represents a break point which separates hysteresis curves. For example curve ABDE in Fig.4(b) represents a counted reversal and points B and E are two break points which mark two uncounted blocks, BCD and EZ, to be dealt with in the subsequent pass. This cycle counting procedure is then repeated, replotting the equivalent relative strains with the reference points being the first point in each block, for example point B for block BCD and point E for block EZ (Fig.4b). The above procedure continues until all the reversals in the history are counted. The multiaxial cycle counting method can be summarised as,

1. Find the peak value of equivalent strain $\epsilon_{eq}(t)$, and denote the corresponding time as t_A.

2. Rearrange the data so that a new data block starts with the major turning point.

3. Find the peak value of equivalent relative strain ϵ^*_{eq} with respect to the first point in the block. A half reversal is counted by combining a sequence of data points where ϵ^*_{eq} is increasing up to the peak value to complete one reversal. A fragmentation of the strain history occurs whenever ϵ^*_{eq} starts to decrease.

4. With the first point of each fragmented data block being the turning point defining ϵ^*_{eq}, repeat step 3 for each block. Further fragmented blocks skipped over during each pass of cycle counting are to be treated in a similar way, until all reversals are counted.

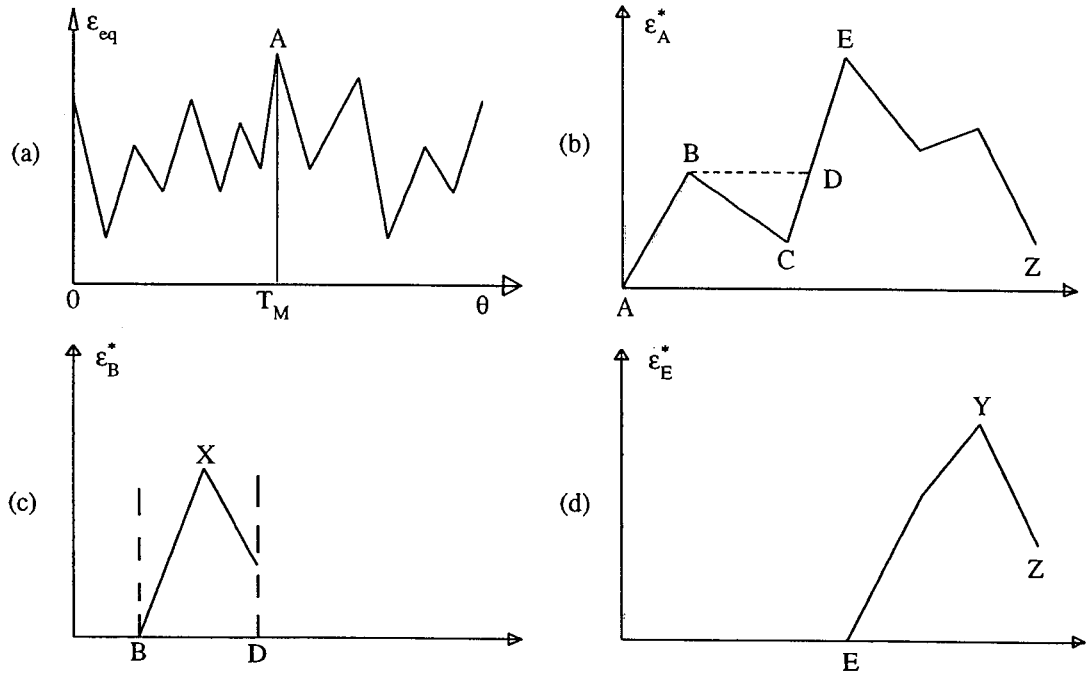

Fig 4: Schematic drawing of cycle counting

The physical basis of the present counting algorithm implies that the method can identify exactly the same turning points and reversals as the rainflow counting in uniaxial random loading. For a single cycle of non-proportional loading, the maximum value of the von MISES

equivalent relative strain is equal to the equivalent strain range defined in the ASME Boiler and Pressure Vessel Code N47-11 [6]. Therefore the ASME code and the rainflow counting become two special cases of the proposed method. One example of non-proportional variable amplitude loading is shown in Fig.5; the simulation of the stress/strain response is shown in Fig.3. One dominant big cycle and 6 smaller reversals are identified. It can be seen that

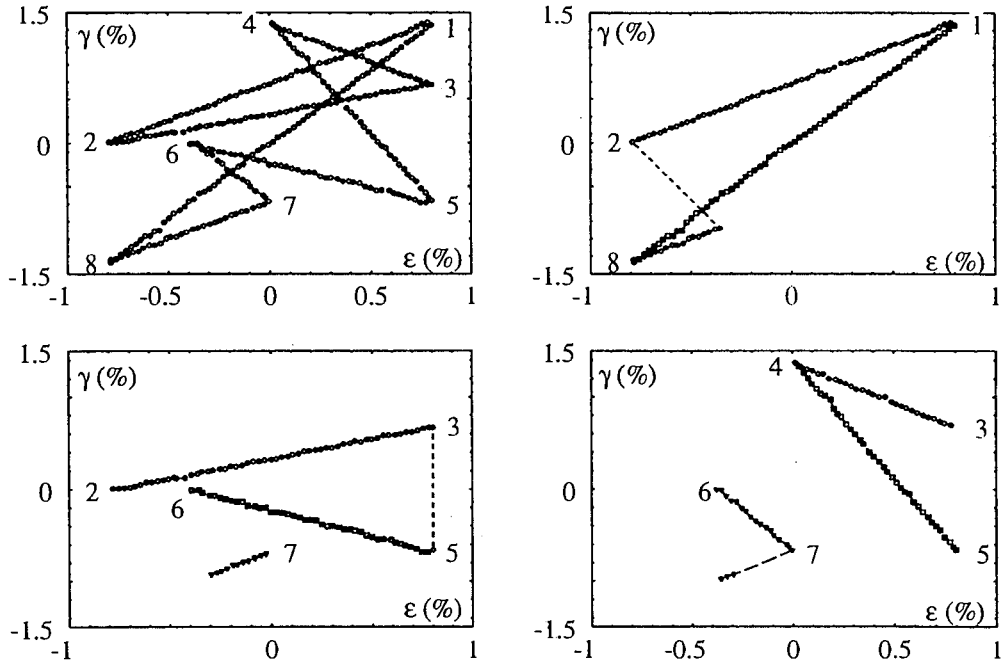

Fig 5: An example of counted reversals of non-proportional variable amplitude loading

the minor reversals do not form closed hysteresis loops, reflecting the change in the straining direction.

Now fatigue damage can be evaluated reversal by reversal. In the present work we will adopt a fatigue damage parameter proposed in [12] to take into account of the non-proportional straining effect on fatigue damage. The effective strain is given as,

$$\hat{\epsilon} \equiv \frac{0.5(\Delta\gamma_{max}) + S(\delta\epsilon_n)}{1+\nu'+(1-\nu')S} = \frac{\sigma'_f - 2\sigma_{n,mean}}{E}(2N_f)^b + \epsilon'_f(2N_f)^c \qquad (18)$$

where $\Delta\gamma_{max}$ and $\delta\epsilon_n$ are the shear strain range and the normal strain excursion between the two turning points of shear strain, respectively, on the plane of maximum shear. The parameter S represents the influence of the normal strain, and for case En15R steel we have $S = 1.38$ for Case A cracking and $S = 0$ for Case B [13]. The other parameters $(\sigma'_f, E, b, \epsilon'_f, c)$ are the uniaxial strain lifetime equation constants. Here the effect of mean stress has been taken into account by using a method analogous to the MORROW mean stress correction, where $\sigma_{n,mean}$ is the mean value of the tensile stress normal to the maximum shear plane. The stresses can be obtained from the constitutive model presented earlier. Because the normal mean stress only affects the first term on the right hand side of equation (18), such correction has little effect in low cycle fatigue region.

The determination of the correct $\delta\epsilon_n$ is of important, since straining path has considerable effect on fatigue damage under non-proportional variable amplitude loading. The proposed

counting method implies that each data point is counted once and only once, which means a big reversal may be formed by segments of loading path which are not continuous with respect to time. Denoting the time instants of a pair of γ_{max} turning points as t_1 and t_2, there are two possible ways to determine $\delta\epsilon_n$. Firstly, one may seek the maximum excursion of the normal strain over the whole continuous period $[t_1, t_2]$,

$$\delta\epsilon_n = \max_{t_1 \le t \le t_2} \epsilon_n(t) - \min_{t_1 \le t \le t_2} \epsilon_n(t) \tag{19}$$

Alternatively, the above procedure may be performed only over the period where the straining path comprises segments of the counted reversal. Obviously the latter method could result in smaller values of normal strain excursion, as fewer data points are used to derive $\delta\epsilon_n$.

Fatigue damage accrued in a loading block is summed up using Miner's linear rule. Fig.6(a) shows a comparison between experimental and predicted lifetime for En15R steel at room temperature. Various loading paths covering proportional and non-proportional variable amplitude loading have been examined in these tests. Both the above methods of determining $\delta\epsilon_n$ are used in the predictions. As expected, the first method yields better correlation to experimental data, whereas the second method underestimates the fatigue damage and the predictions are slightly on the non-conservative side. Some experimental data of 304 stainless steel at high temperature were taken from the literature [14], from which detailed explanation of the loading paths can be found. A total of fourteen different straining paths have been tested. The predicted and experimental lifetime are shown in Fig.6(b). It can be seen that most predictions are within a scatter band of a factor of two, which is considered acceptable.

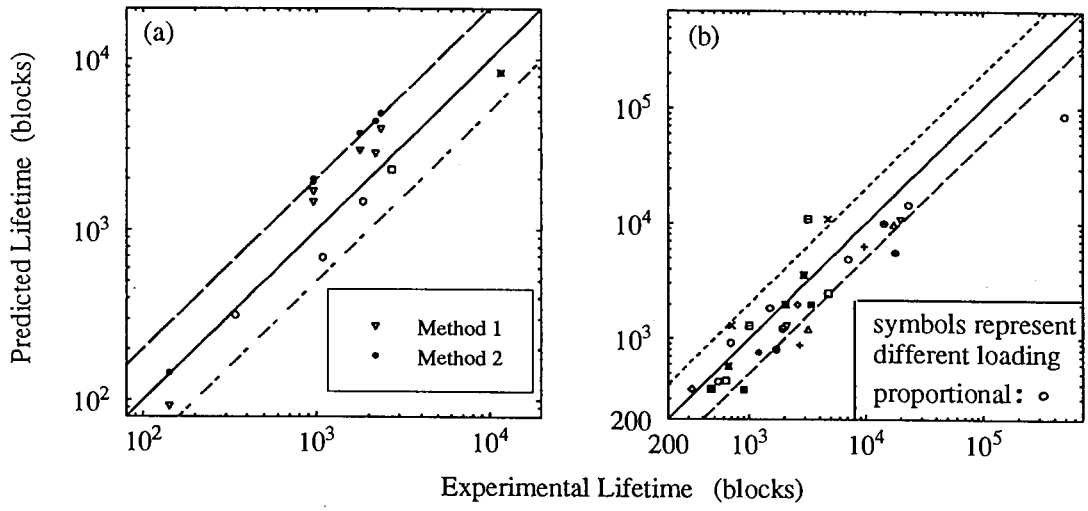

Fig 6: Comparison between experimental and predicted lifetime; (a) En15R steel at room temperature (b) 304 stainless steel at high temperature ($T = 550^0$C)

4 DISCUSSION AND CONCLUSIONS

In constructing the cycle counting method, it was assumed that a peak equivalent stress would correspond to the peak value of equivalent strain related through equation (13); obviously mean stress relaxation is not considered. The major turning points determined by the

proposed method using equations (16) and (17) may not necessarily give maximum range of equivalent stress (and vice versa). For example when a large mean strain is present, the maximum peak value of ϵ_{eq} may not correspond to the maximum value of σ_{eq}, as the mean stress may be fully relaxed after a few blocks.

One alternative method would be to identify the two data points between which the equivalent relative strain range attains peak value, i.e.,

$$\Delta\epsilon_{eq} = \max_{0\le t_A\le\theta}\left[\max_{0\le t_B\le\theta}\epsilon_{eq}(\epsilon_{ij}^{A}-\epsilon_{ij}^{B})\right] \tag{20}$$

where times t_A and t_B will be the two major turning points, and between these points equivalent relative stress may also achieve a higher peak value. However, this method requires a double maximization procedure and may involve more computation. In the present investigation, since most of tests were conducted under strain controlled conditions with the ratio of minimum to maximum strains being -1, the two methods would yield the same results. Further work is, however, needed to evaluate the merits of these two methods for other multiaxial random loading histories.

The following conclusions can be drawn from the present study,

1. A rate-independent plasticity model and a memory rule have been proposed, and a satisfactory description of the inelastic deformation response under complex loading has been achieved.

2. The effect of multiaxial loading history has been successfully incorporated in the constitutive relationship through a scalar memory parameter.

3. The proposed one-dimensional memory model has been shown to be capable of simulating the inheritance and erasing of memories under complex loading history.

4. A multiaxial cycle counting method has been proposed. A correlation for endurance within a factor of two has been achieved, which demonstrates the capability of the method.

5. The proposed general cycle counting method reduces to rainflow cycle counting in uniaxial loading and to the ASME code for simple non-proportional loading cycles.

Acknowledgement— The authors thank the sponsors of BRITE/EURAM programme BR/EU 3051, contract No. 0099, for financial support for the project.

REFERENCES

1. Mróz, Z. (1967) On the Description of Anisotropic Work-Hardening, *J. Mech. Phys. Solids.*, **15**, 163.

2. Krieg, R. D. (1975) A Practical Two-surface Plasticity Theory, *J. of Applied Mechanics*, **42**, pp.641–646.

3. Dafalias, Y. F. and Popov, E. P. (1976) Plastic Internal Variables Formalism of Cyclic Plasticity, *J. of Applied Mechanics*, **43**, pp.645–651.

4. Chaboche, J. L. (1986) Time-Independent Constitutive Theories for Cyclic Plasticity, *Int. J. Plasticity*, **2**, No.2, pp.149–188.

5. Proceedings of International Conference on Multiaxial Plasticity, Sept. 1992, LMS Cachan, Paris.

6. Criterion for Design of Elevated Temperature Class I Components in Section III, Division 1 of ASME Boiler and Pressure Vessel Code, Case Code N47, ASME, 1976.

7. Matsuishi, M. and Endo, T. (1968) Fatigue of metals subjected to varying stress, presented to *Japan Society of Mechanical Engineers*, Fukuoka, Japan, March 1968.

8. Burns, A. (1956) Fatigue Loadings in Flight: Loads in the Tailplane and Fin of a Varsity, *Aeronautical Research Council Technical Report*, C.P. 256, London.

9. Wang, C. H. and Brown, M. W. (1992) Experimental and theoretical study of the deformation behaviour of En15R steel under multiaxial loading, *International Conference on Multiaxial Plasticity*, Paris, France, Sept. 1992.

10. Prager, W. (1956) A new method of analyzing stresses and strains in working hardening plastic solids, *ASME J. Appl. Mechanics*, **78**, p.493.

11. Armstrong, P. J. and Frederick, C. O. (1966) A mathematical representation of the multiaxial Bauschinger effect, *CEGB Report RD/B/N731*, Berkeley Nuclear Laboratories.

12. Wang, C. H. and Brown, M. W. (1993) A path-independent parameter for fatigue under proportional and non-proportional loading, submitted to *Fatigue Fract. Engng. Mater. Struct.* for publication.

13. Brown, M. W. and Miller, K. J. (1973) A theory for fatigue failure under multiaxial stress–strain conditions, *Proceedings of the Institution of Mechanical Engineers*, **187**, 65/73, pp.745–755.

14. Ohnami, M. and Sakane, M. (1992) Design criteria for multiaxial creep-fatigue, presented at the *ASTM Creep Conference*, Orlando, Florida, USA, 1992.